PERGAMON

International Journal of Heat and Mass Transfer 42 (1999) 3943–3958

International Journal of HEAT and MASS TRANSFER

www.elsevier.com/locate/ijhmt

Thermophysical property measurements of building materials in a periodic state

Omar Douzane*, Jean-Marc Roucoult, Thierry Langlet

Laboratoire des Transferts et Réactivité dans les Milieux Condensés, Université de Picardie Jules Verne, IUT Génie Civil, Avenue des facultés, 80025 Amiens Cedex, France

Received 20 April 1998; received in revised form 20 February 1999

Abstract

A simplified experimental device and a theoretical model used for measurement of thermal diffusivity and effusivity of building materials are presented. This study is an extension of methods which employ a periodic signal, performed in our laboratory. The impact of contact thermal resistances between the device's different components and the role played by the presence of the heat flowmeter have been studied. Experimental results obtained for two materials with different thermal properties are finally presented. © 1999 Elsevier Science Ltd. All rights reserved.

1. Introduction

Thermal diffusivity and effusivity are two essential characteristics of the behavior of materials in an unsteady state. Experimental techniques that allow determining their values are based upon an identical principle: a signal is produced on the entrance face of a studied material sample, and the thermal response is then recorded at another point on the material. This signal is generally an impulse, a periodic function or a step function.

Impulse methods with a typical flash are well-suited to homogeneous materials and small thicknesses, such as those of plasma deposits [1,2]. In contrast, for civil engineering materials which exhibit a certain degree of heterogeneity, it is suggested that the step or periodic methods used be allowed to generate this entrance signal on the largest surface. These methods differ in terms of the temperature range over which they are applicable, their ease of implementation, the degree of automation and their speed in providing results. Step methods, by virtue of their speed, can be used over other methods for controlling manufacturing processes [3,4].

Methods that incorporate modulation enable creating a periodic temperature differential in a sample thanks to a lamp-to-arc modulation; it is well-suited for very high temperature measurements [5,6].

The periodic state methods that the authors have been developing in their laboratory over the past ten years are adapted to the materials presenting grains whose larger dimension is not greater than 1/4 of the thickness of the sample as specified in the norm NF X 10-021 [7]. Elements of the experimental set-up are identical to those used in the standardized hot plate-method device [7,8]. The principle behind these methods is to generate calorific flows on the extreme faces of a few samples by using hot plates and then to record both surface temperature signals and flow once the periodic state has been established. The application of a Fourier-series decomposition of these signals leads

* Corresponding author. Tel.: +33-3-22-53-40-43; fax: +33-3-22-95-17-51.

E-mail address: Omar.Douzane@iut.u-picardie.fr (O. Douzane)

0017-9310/99/$ - see front matter
PII: S0017-9310(99)00076-9

Nomenclature

a	thermal diffusivity [$m^2\ s^{-1}$]
A	damping
b	thermal effusivity [$J\ s^{-1/2}\ m^{-2}\ K^{-1}$]
C	calorific capacity [$J\ K^{-1}\ m^{-2}$]
D	phase shift
e	thickness of the sample [m]
e^*	penetration depth [m]
H	dimensionless parameter defined in Eq. (26)
k	thermal conductivity [$W\ m^{-1}\ K^{-1}$]
P	period of the signal [s]
r	corrective coefficient of the heat flowmeter defined in Eq. (25)
Rc	thermal contact resistance between the 2 samples [$m^2\ K\ W^{-1}$]
T	temperature field [°C]
$\|T\|$	amplitude of the temperature signal [°C]
t	time [s]
x, y	abscissa [m]

Greek symbols

α, β	coefficients of the trigonometric functions of the Fourier series
δ	dimensionless parameter $= e_s/e_i + e_s$
ψ	shift between flow and temperature signals
φ	surfacic flow [$W\ m^{-2}$]
$\|\varphi\|$	amplitude of the flow signal [$W\ m^{-2}$]
η	dimensionless parameter defined in Eq. (5)
ω	pulsation of the signal [s^{-1}]

Subscripts

f	heat flowmeter
i	lower sample
l	air jet
m	average
s	upper sample
cs	contact face of the upper sample
ci	contact face of lower sample

to determining both the thermal diffusivity and effusivity.

The various devices developed can be differentiated both by the manner in which their components are assembled and by the nature of the calorific flow functions generated. A first-generation device, called symmetrical, possesses a thermal as well as a geometrical symmetry plan [9]. The difficulties encountered with respect to the thermal symmetry have led us to renounce this type of symmetry and instead to utilize

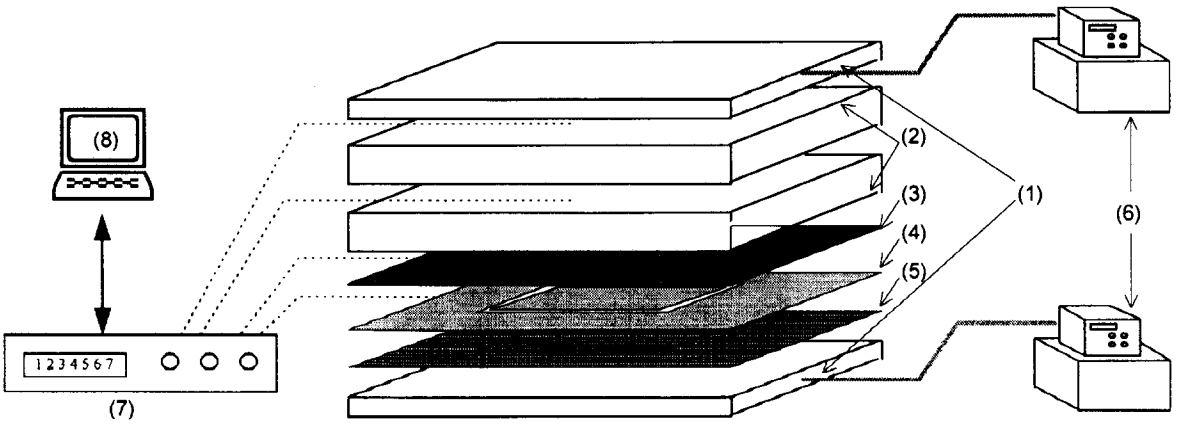

(1) : exchanging plate (4) : thermopile (7) : data acquisition central

(2) : samples (5) : hot plate (8) : computer

(3) : heat flowmeter (6) : thermostat

Fig. 1. Schematic diagram of the experimental apparatus.

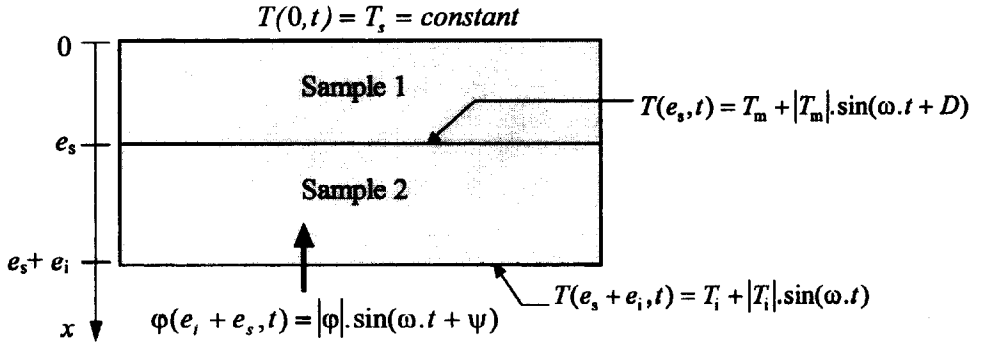

Fig. 2. Description of the thermal model.

the in-source results from a non-symmetrical model [10].

Recently, a 'lighter' device has been developed by renouncing the thermal and geometrical symmetries [11]. With this apparatus, a calorific flow is generated on the basis of dual-pile samples, while the upper face of the samples involved is maintained at a constant temperature.

In this article, it is planned to achieve the work that has been laid out with the help of this new apparatus.

2. Experimental set-up

The experimental apparatus, as shown in Fig. 1, is made up of similar elements to those used for the thermal conductivity measurement by the standardized hot-plate method.

The system is composed of:

- one hot plate (5) consisting of a square central zone (250 × 250 mm) and a guarded zone with an external dimension of 500 × 500 mm. The hot plate generates a periodic calorific flow. The peripheral resistance allows producing unidirectional incoming heat flow on the lower face of the samples,
- two samples of the studied material (2),
- two exchanging plates (1), maintained at constant temperature thanks to a heat exchanging fluid (6), which serve to set thermal levels on both the lower and upper faces of the device,
- one thermopile (4), made up of 20 thermocouples in series laid out in an alternating arrangement between the central zone and the guarded zone, enables measuring the temperature differential between these two zones,
- one calorific flowmeter (3) which allows recording the rise in heat flow generated by the hot plate in the lower sample. This sensor is of the 'tangential gradient' type with coplanar electrical couple junctions [12]. It has been previously covered by a sheet of aluminum so as to render its calibration coefficient independent of the contact material [13]. Characteristics of this particular component, along with its influence on the determination of thermal effusivity, are further developed in Section 6,
- surface temperatures are measured with the help of thermocouples ('T' type) positioned, for hard materials, in grooves etched onto the surface of the samples, and
- a lateral insulation, applied with vermiculite, which limits thermal releases occurring at the periphery of the device. Such releases are generally located at the level of the hot plate and do not serve to substantiate some of the hypotheses of unidirectional flow within the samples, as a recent study would have suggested [14].

The entire set-up is then placed into a tightening device so as to reduce the thermal contact resistance between the various components of the assembly.

Once the state has been established, a database is compiled from records of the measurements taken, over the duration of a single period, of the temperature on the lower face, the temperature on the contact face and incoming flow by the lower face of the samples. These different signals are then decomposed into a Fourier series; this will ultimately allow determining the thermal diffusivity and effusivity of the studied material.

3. Formulation of the problem

3.1. The thermal model selected

Considering the samples and the geometry precautions taken in order to limit the lateral releases, the

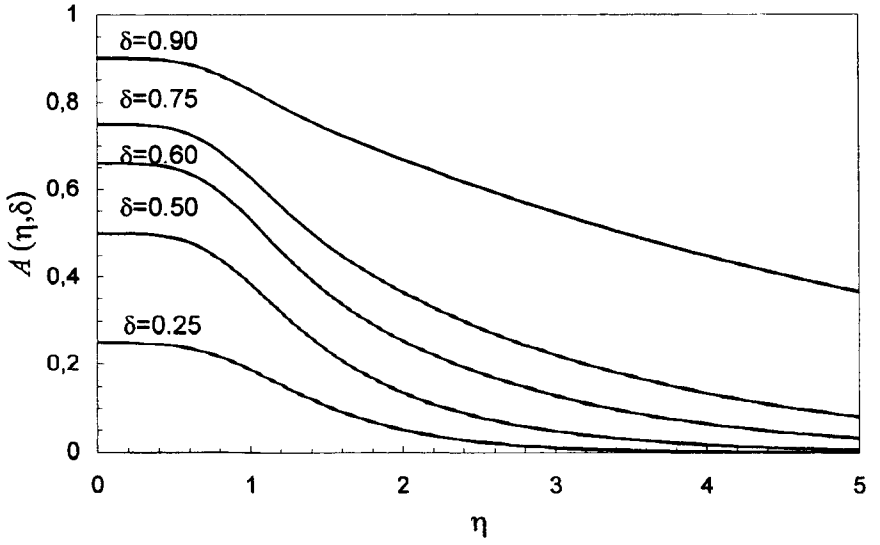

Fig. 3. Evolution of the damping as a function of η for different thickness ratios.

unidirectional heat transfer model described in Fig. 2 have been selected. The unidirectional character of the heat transfer is verified thanks to the presence of a thermopile on the lower face of the device (Fig. 1) in accordance with the norm of the hot plate method [7]. Indeed, these thermopiles, placed in the device, allows one to adjust experimental parameters in order to have a null temperature difference between the two zones (the central zone and the guarded zone).

The calorific flow is generated by the hot plate to the abscissa e_i+e_s, which corresponds to the lower face of the sample couple. The thicknesses of the upper and lower samples are denoted e_s and e_i, respectively, and the dimensionless parameter $\delta=(e_s/e_i+e_s)$ has been used throughout the remainder of the article.

The temperature field of the sample couple is denoted $T(x, t)$ and the flow density $\varphi(x, t)$.

The system of equations governing this model is as follows:

$$\frac{\partial T(x,t)}{\partial t}=a\frac{\partial^2 T(x,t)}{\partial x^2} \tag{1}$$

$$T(0,t)=T_s=\text{constant} \tag{2}$$

$$T(e_i+e_s)=T_i+\mid T_i\mid \sin(\omega t) \tag{3}$$

with: $\omega=\sqrt{2\pi}/P$, pulsation of the signal; P, period; a, the thermal diffusivity of the material.

The established periodic state, which represents the solution to this system of equations, is given by the following expression (4):

$$\tilde{T}(x,t)=A(\eta,x)\mid T_i\mid \sin(\omega t+D(\eta,x)) \tag{4}$$

where $A(\eta, x)$ and $D(\eta, x)$ represent the damping and the phase shift, respectively, for the signal in terms of temperature $\tilde{T}(x, t)$ in comparison with the signal $\tilde{T}(e_i+e_s, t)$. They are expressed as a function of the dimensionless parameter η, as given in (5):

$$\eta=\frac{e_i+e_s}{2}\sqrt{\frac{\omega}{2a}}=\frac{e_i+e_s}{2}\frac{1}{e^*} \tag{5}$$

with: e^* the penetration depth of the thermal signal into the material.

The expressions, in terms of $x=e_s$ for both the damping and phase shift are given by Eqs. (6) and (7), respectively, as a function of either the ratio δ or the penetration depth e^*:

$$A(\eta,\delta)=\sqrt{\frac{\mathrm{ch}(4\eta\delta)-\cos(4\eta\delta)}{\mathrm{ch}(4\eta)-\cos(4\eta)}}=\sqrt{\frac{\mathrm{ch}\left(\frac{2e_s}{e^*}\right)-\cos\left(\frac{2e_s}{e^*}\right)}{\mathrm{ch}\left(2\frac{e_s+e_i}{e^*}\right)\cos\left(2\frac{e_s+e_i}{e^*}\right)}}=\frac{\mid T_m\mid}{\mid T_i\mid} \tag{6}$$

$$D(\eta,\delta)=\mathrm{Arctg}\left(\frac{\mathrm{tg}(2\eta\delta)}{\mathrm{th}(2\eta\delta)}\right)-\mathrm{Arctg}\left(\frac{\mathrm{tg}(2\eta)}{\mathrm{th}(2\eta)}\right)=\mathrm{Arctg}\left(\frac{\mathrm{tg}\left(\frac{e_s}{e^*}\right)}{\mathrm{th}\left(\frac{e_s}{e^*}\right)}\right)-\mathrm{Arctg}\left(\frac{\mathrm{tg}\left(\frac{e_s+e_i}{e^*}\right)}{\mathrm{th}\left(\frac{e_s+e_i}{e^*}\right)}\right) \tag{7}$$

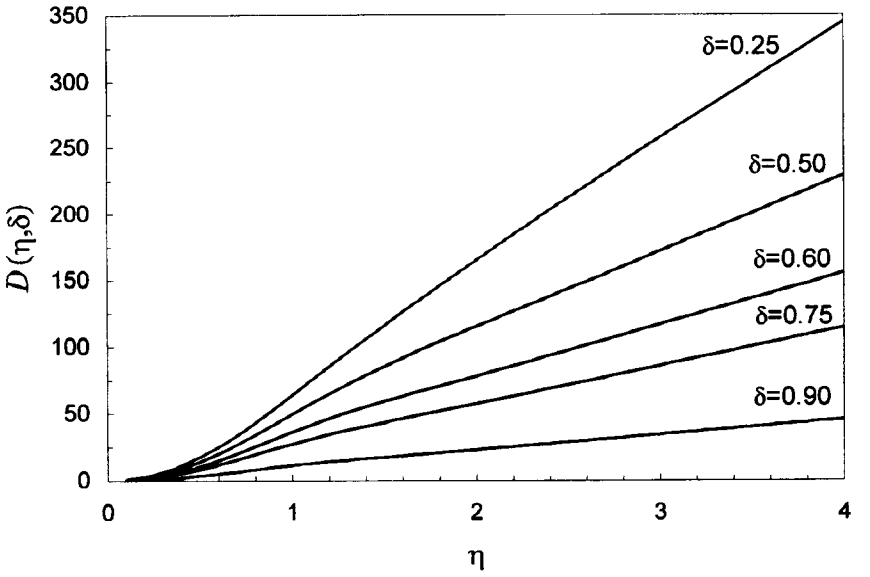

Fig. 4. Evolution of the phase shift as a function of η for different thickness ratios.

For small values of η, expression (6) can be approximated by: $A(\eta, \delta)=\delta$ and expression (7) tends towards zero. Furthermore, at each instant, the temperature profile of the samples is nearly linear. Samples exhibit a behavior that is indicative of a medium of extremely small thickness in which perturbations are transmitted quasi-instantaneously to all points. It is therefore impossible to determine the thermal diffusivity in this particular case. For large values of η, the samples exhibit a practically semi-infinite behavior; heat transfer is thus localized primarily near the lower face of the sample couple. If the ratio e_s/e^* is very less than e_s+e_i/e^*, it then becomes, in this case as well, difficult to obtain the thermal diffusivity.

Figs. 3 and 4, in which variation curves of both expressions (6) and (7) are presented as a function of η, serve to illustrate the previous remarks. It can be observed in Fig. 3 that the damping A decreases as η increases for different thickness ratios δ. This damping gets even further reduced as a result of the thickness of the upper sample being less than that of the lower sample.

The expression of the surfacic flow is given by:

$$\tilde{\varphi}(x, t) = | \varphi | \sin(\omega t + \psi) \tag{8}$$

with ψ representing the shift between signals $\varphi(x, t)$ and $\tilde{T}(x, t)$, and $|\varphi|$ the amplitude of the signal. Their expressions are given in Eqs. (9) and (10), respectively, with respect to η:

$$\psi(\eta, e_i + e_s) = \frac{\pi}{4} - \mathrm{Arctg}\left(\frac{\mathrm{tg}(2\eta)}{\mathrm{th}(2\eta)}\right) + \mathrm{Arctg}(\mathrm{th}(2\eta)\mathrm{tg}(2\eta)) \tag{9}$$

$$| \varphi | = | T_i | b\sqrt{\omega}\sqrt{\frac{\mathrm{ch}(4\eta) + \cos(4\eta)}{\mathrm{ch}(4\eta) - \cos(4\eta)}} \tag{10}$$

with b the thermal effusivity of the material.

For small values of the parameter η, expression (10) can be approximated by

$$| \varphi | = | T_i | \frac{k}{e_i + e_s},$$

where k is the thermal conductivity of the tested material. It is naturally found that the behavior exhibited at the 'middle of the extremely small thickness' will not enable determining the thermal effusivity. In contrast, for η values of greater than 1.8, expression (10) turns out to be independent of η; $| \varphi | = | T_i | b\sqrt{\omega}$.

3.2. Application to the determination of thermal diffusivity and effusivity

In the established state, the decomposition of the measured periodic signals $\tilde{T}(e_i+e_s, t)$ and $\tilde{T}(e_s, t)$ into a Fourier series allows determining, with the help of the fundamental, both the damping $A(\eta, \delta)$ and the phase shift $D(\eta, \delta)$, as given by expressions (11) and (12):

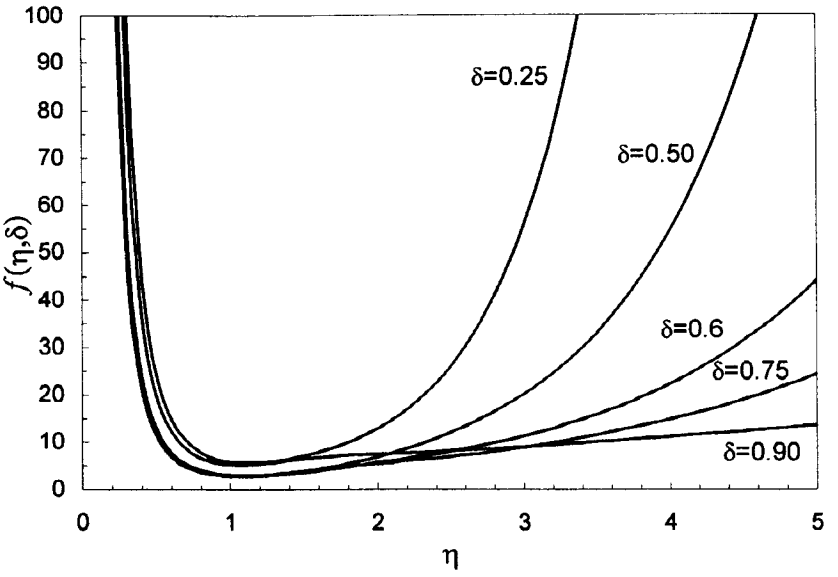

Fig. 5. Evolution of the function $f(\eta, \delta)$.

$$A(\eta, \delta) = \sqrt{\frac{\alpha_m^2 + \beta_m^2}{\alpha_i^2 + \beta_i^2}} \tag{11}$$

$$D(\eta, \delta) = \mathrm{Arctg}\left(\frac{\beta_m}{\alpha_m}\right) - \mathrm{Arctg}\left(\frac{\beta_i}{\alpha_i}\right) \tag{12}$$

with (α_m, β_m) and (α_i, β_i) representing the coefficients of the trigonometric functions appearing in the decomposition into a Fourier series of experimental signals $T(e_s, t)$ and $T(e_i + e_s, t)$.

The experimental values obtained for $A(\eta, \delta)$ and $D(\eta, \delta)$ have led, in conjunction with the curves displayed in Figs. 3 and 4, to two values for η. Their utilization makes it possible to identify the thermal diffusivity, thanks to expression (5).

Similarly, use of the flow signal enables, by employing expression (10), identifying the thermal effusivity of the studied material. Nevertheless, in order to incor-

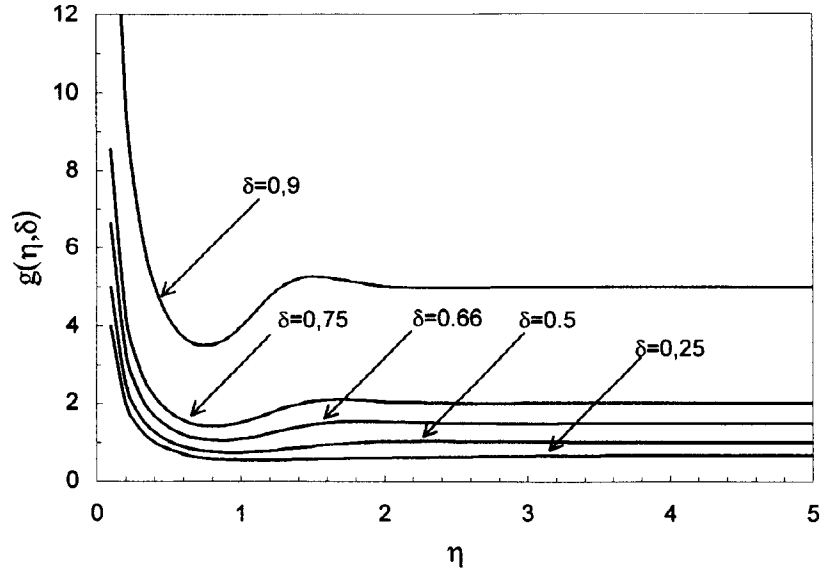

Fig. 6. Evolution of the function $g(\eta, \delta)$.

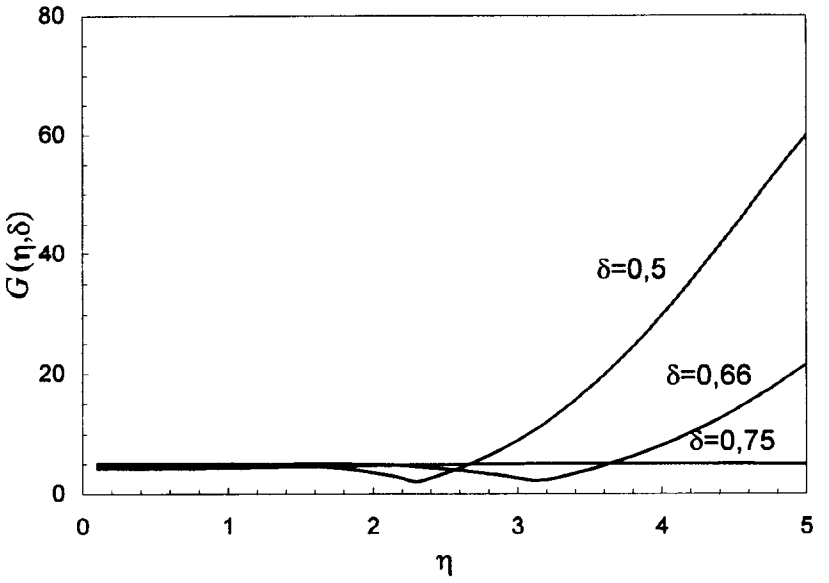

Fig. 7. Evolution of the function $G(\eta, \delta)$.

porate the presence of the heat flowmeter, it is essential to apply a correction factor to the obtained value (see Section 6).

Initial analyses, conducted on the basis of theoretical expressions, have revealed that this method was not applicable over the range of small η values and that only b could be determined for the large η values. In light of previous remarks, it will be attempted to identify, in the next section, the effective range of η values for determining the magnitudes of thermophysical properties.

4. Choice of experimental parameters

4.1. Identification of the most advantageous conditions for determining the magnitudes of thermophysical properties

The level of uncertainty encountered in determining η values by solving the system of Eqs. (6) and (7) (or by applying the curves in Figs. 3 and 4) is given in accordance with the experimental uncertainty derived from expressions (13) and (14):

$$\Delta\eta = \Delta A(\eta, \delta) f(\eta, \delta) \tag{13}$$

$$\Delta\eta = \Delta D(\eta, \delta) g(\eta, \delta) \tag{14}$$

In Fig. 5, the shape of the function $f(\eta, \delta)$ has been plotted for various values of the ratio δ. These curves display a minimum at $\eta \approx 1$, and the two unusable zones mentioned in Section 3 are also apparent.

It can be noted that for the studied configurations, only three—$\delta = 0.50$, 0.66 and 0.75—allow satisfying $f(\eta, \delta) \leq 5$ for η values lying between 0.7 and 1.8.

In Fig. 6, the shape of the function $g(\eta, \delta)$ is presented. From a η value equal to 0.5, all of the configurations being studied herein, except that for which $\delta = 0.90$, do satisfy the condition: $g(\eta, \delta) \leq 2$. This therefore proves that among the studied configurations, the most promising are: $\delta = 0.5$, 0.66 and 0.75. Moreover, it would be most effective to position this value in the range of [0.7–1.8] by seeking as a priority those η values which tend towards 1 in order to minimize uncertainty in the determination of the desired thermophysical characteristics. In the following section, it will be ascertained whether or not the interval [0.7–1.8] for the parameter η is equally as effective with respect to the experimental program.

4.2. Uncertainty in the experimental program

On the basis of expressions (11) and (12), the uncertainties present in the experimental determination of both the damping and phase shift are obtained from Eqs. (15) and (16), respectively, in which the parameter η has been introduced through expressions (6) and (7):

$$\Delta A(\eta, \delta) = F(\eta, \delta) \frac{\Delta T}{|T_i|} \tag{15}$$

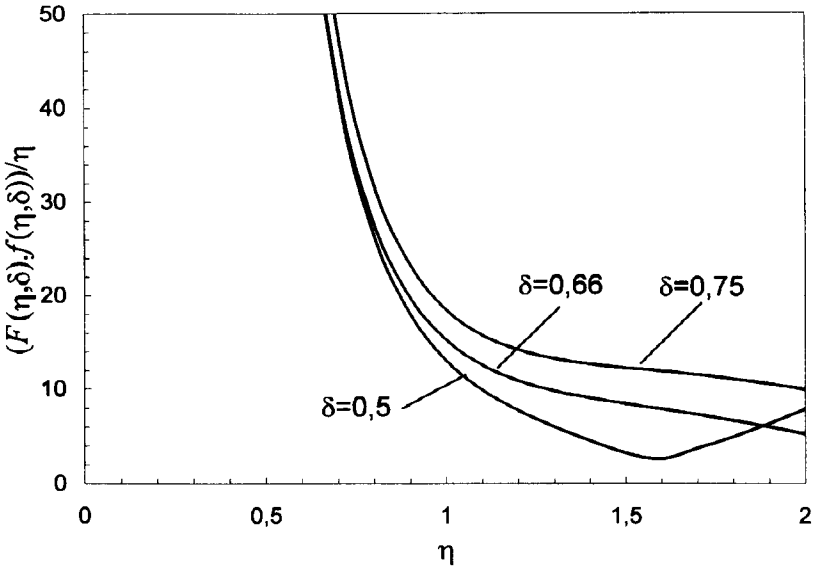

Fig. 8. Evolution of $F(\eta\,\delta)f(\eta,\delta)/\eta$ as a function of η for different values of δ.

$$\Delta D(\eta,\delta) = G(\eta,\delta)\frac{\Delta T}{|T_i|} \tag{16}$$

with ΔT representing the uncertainty for each temperature measurement.

Fig. 7 displays the evolution of the function $G(\eta,\delta)$ for the three indicated values of δ. It can be noted that for large values of η, the uncertainty $G(\eta,\delta)$ increases rapidly. The material's infinite semi-wall behavior, as pointed out in Section 3, has been detected in this instance; the interface of the two test tubes, at too great a distance from the lower face (value of δ is small), barely receive the signal being emitted by the hot plate. The interval [0.7–1.8] selected in Section 4.1 corresponds to a zone of weak amplitude for the function $G(\eta,\delta)$, which is of distinct experimental interest.

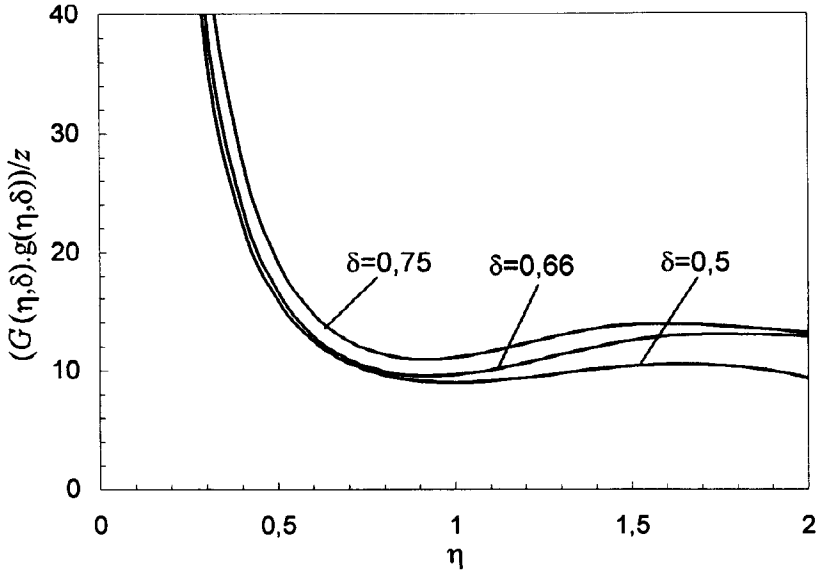

Fig. 9. Evolution of $G(\eta,\delta)g(\eta,\delta)/\eta$ as a function of η for different values of δ.

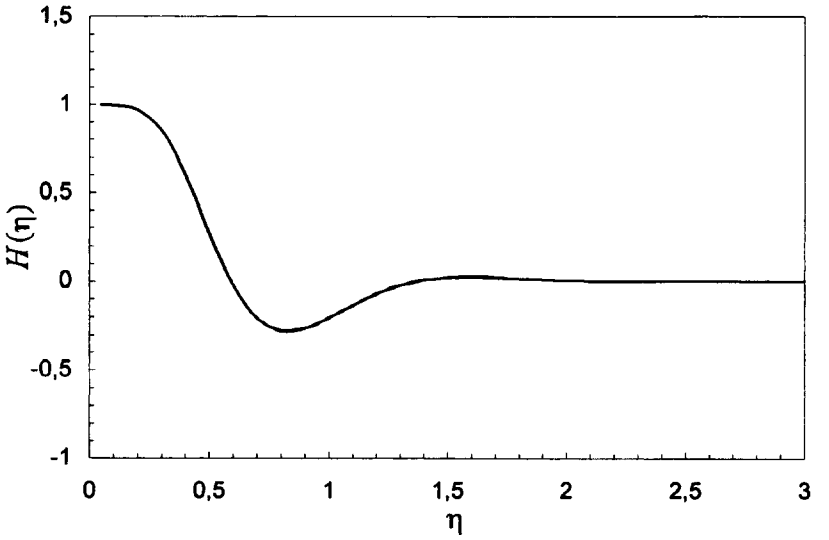

Fig. 10. Evolution of $H(\eta)$ as a function of η ($\delta = 0.5$).

The same conclusion can be drawn from a study of the function $F(\eta, \delta)$. The determination of thermal diffusivity from the use of damping thus proves to be more effective from an experimental standpoint than that involving the phase shift. The configuration with a δ value of 0.50, i.e. when the two test tubes have the same thickness, turns out to be the most effective.

4.3. Uncertainty with respect to the determination of thermal diffusivity and effusivity

The relative uncertainty of the thermal diffusivity is obtained from expressions (17) and (18) by using the damping and the phase shift, respectively:

$$\frac{\Delta a}{a} = 2\frac{F(\eta, \delta) f(\eta, \delta)}{\eta} \frac{\Delta T}{|T_i|} \tag{17}$$

$$\frac{\Delta a}{a} = 2\frac{G(\eta, \delta) g(\eta, \delta)}{\eta} \frac{\Delta T}{|T_i|} \tag{18}$$

In Figs. 8 and 9, the functions

$$\frac{F(\eta, \delta) f(\eta, \delta)}{\eta} \quad \text{and} \quad \frac{G(\eta, \delta) g(\eta, \delta)}{\eta}$$

have been plotted. The configuration with $\delta = 0.5$ is revealed to be the most effective for both of the determinations. By means of the phase shift, for

$$\eta \in [0.7\text{–}1.8], \quad \frac{\Delta a}{a} = 10\frac{\Delta T}{|T_i|}$$

is obtained. In contrast, by employing the damping, the relative uncertainty of the thermal diffusivity is lower for $\eta \in [1.05\text{–}1.8]$.

The uncertainty in the determination of thermal effusivity can be obtained by expression (19):

$$\frac{\Delta b}{b} = H(\eta)\frac{\Delta \eta}{\eta} + \frac{\Delta |\varphi|}{|\varphi|} + \frac{\Delta |\theta_1|}{|\theta_1|} \tag{19}$$

The shape of the function $H(\eta)$ is shown in Fig. 10. For a low penetration depth of the signal, which corresponds herein to $\eta \geq 1.8$, the function $H(\eta)$ is just about zero. The thermal effusivity b then becomes independent of η, which provides for the highest-quality determination.

In conclusion, except for small values of η, it will always be possible to determine a thermal characteristic of the dynamic state. The range $\eta \in [1.05\text{–}1.8]$ will allow identifying the thermal diffusivity which displays a minimal uncertainty, by using the temperature signal's damping rather than its phase shift. For 5-cm thick test tubes, this would place the period of the emitted signal inside the interval [0.5–1.8 h] for the marble and [0.25–1 h] for the polystyrene.

5. Influence of contact resistance

The assembly of the various components within the experimental set-up can serve to introduce contact resistance, primarily at those interfaces where the thermocouples are attached. In order to study their influence on results, the initial model has been modified by introducing a contact resistance Rc either on the interface of the two test tubes or on the upper exchanging plate—upper sample interface.

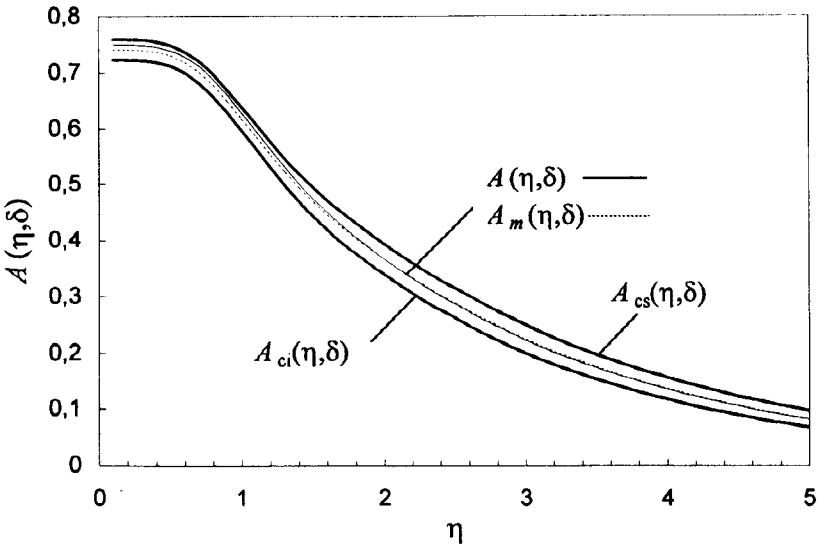

Fig. 11. Influence of the contact resistance at the interface of 2 samples on damping as a function of the parameter η ($\delta = 0.5$).

5.1. Case of a thermal contact resistance between the two samples

The resolution of this new model incorporates a dimensionless parameter $Rc^* = Rc(k/e)$, where k is the thermal conductivity of the tested material and Rc the contact resistance between the two samples. This model leads to developing expressions both for the damping $A_{cs}(\eta, \delta)$ and $A_{ci}(\eta, \delta)$ of the signal $T(e_i + e_s, t)$ on either side of the contact resistance and for $D_{cs}(\eta, \delta)$ and $D_{ci}(\eta, \delta)$ which correspond to the phase shifts. The introduction of experimental values into these expressions enables making a determination of Rc^*. The numerous tests conducted on marble samples have shown that Rc^* is positioned in the interval [0.015–0.04], which corresponds to a contact resistance value of less than 0.008°C m^2/W for the 5-cm thick test tubes. In the case of the polystyrene, this resistance

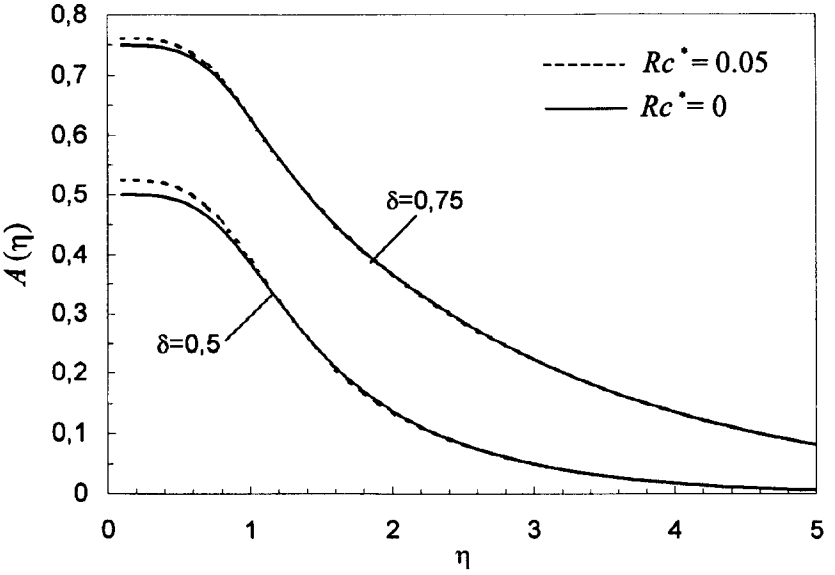

Fig. 12. Damping as a function of the parameter η ($\delta = 0.5$ and $\delta = 0.75$).

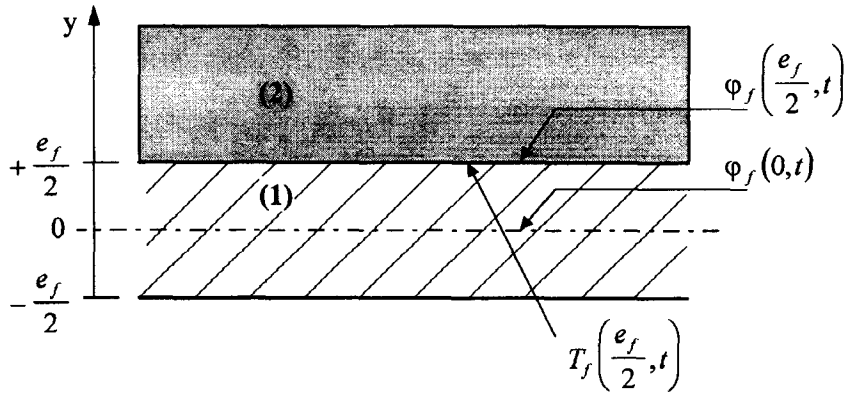

Fig. 13. Measure of the flow and temperature on the lower sample face.

is once again lower, which is why only the results concerning the marble will be mentioned in this section.

In the case of the configuration with $\delta=0.5$, Fig. 11 presents the results concerning the unfavorable case of $Rc^*=0.05$. In this figure, the curves $A_s(\eta, \delta)$ and $A_i(\eta, \delta)$ have been plotted; the curve $A(\eta, \delta)$, which is associated with the case of a zero resistance, has also been graphed. A comparison of the curve $A(\eta, 0.5)$ with the average curve defined by $A_m(\eta, \delta) = \frac{1}{2}(A_{cs}(\eta, 0.5) + A_{ci}(\eta, 0.5))$ reveals that these two curves are practically indistinguishable; their maximum deviation is 0.1%. Similarly, a maximum deviation of 0.1% has been recorded between the curve $D(\eta, 0.5)$ and the average curve defined by $D_m(\eta, \delta) = \frac{1}{2}(D_{cs}(\eta, 0.5) + D_{ci}(\eta, 0.5))$.

In the configuration with $\delta=0.5$, one can therefore eliminate the measurement of the contact resistance by continuing to apply results that correspond to the case of a zero contact resistance, provided the average of the readings recorded by the two thermocouples placed to the right of the interface on each sample has been used.

In contrast, this process can no longer be applied once the ratio δ exceeds 0.5. For $\delta=0.75$, for example, the curves $A_m(\eta, 0.75)$ and $A(\eta, 0.75)$ are then no longer indistinguishable; a deviation reaching as high as 2% has been recorded. This result can be explained by means of a simple analysis: since the air jet is purely resistive, the curve thereby corresponds to the damping in the middle of the air jet. If the equivalent thickness of the air jet were denoted e_L, such that $Rc=(e_L/k)$, a configuration with $\delta=e_s/(e_s+e_i)$ corresponds in fact to a configuration with

$$\delta^* = \frac{e_s + e_L/2}{e_s + e_i + e_L} = \delta + \frac{(1/2 - \delta)e_L}{e_s + e_i + e_L}.$$

Only the configuration $\delta=0.5$ allows $\delta^*=\delta$, which explains why curves $A(\eta, 0.5)$ and $A_m(\eta, 0.5)$ are almost indistinguishable. As the value of δ grows further from 0.50, $A(\eta, \delta)$ and $A_m(\eta, \delta)$ will tend to grow further apart; they will become indistinguishable only when the behavior of the semi-infinite wall (large η value) has been identified.

The configuration corresponding to a $\delta=0.5$ thus makes it possible to continue utilizing the model presented without taking the contact resistance into account; the error involved in determining η with the help of curves $A(\eta)$ and $D(\eta)$ remains less than 0.1%.

5.2. Case of a contact resistance between the upper sample and the exchanging plate

The presence of this contact resistance means that the constant-temperature hypothesis can no longer be satisfied on the upper face of the sample couple. The new model exhibits the dimensionless parameter $Rc^*=Rck/(e_s+e_s)$. In Fig. 12, the curves $A(\eta, 0.5)$, associated with $Rc^*=0$ and $Rc^*=0.05$ have been compared. A sizable deviation between the two curves for large values of the signal's penetration depth (small η value) can be observed, yet this deviation quickly becomes small for $\eta \geq 1$ (maximum deviation of 1.3%). The comparison with the configuration in which $\delta=0.75$ yields smaller deviations between the results from the two models (a maximum deviation of 0.7%).

In a similar analysis as the one presented in Section 5.1, the following is obtained:

$$\delta^* = \delta + \frac{(1-\delta)}{e_s + e_i + e_L},$$

which demonstrates that the deviation between the two models decreases as δ increases.

A similar set of conclusions can be drawn with respect to the phase shift, albeit with less sizable deviations between the two models.

For example, for a δ value of 0.50, neglecting this contact resistance could cause an error in the determination of η that is larger than the one mentioned in the preceding section. It is therefore recommended herein to remove the thermocouple fixed on the upper face of the sample couple in order to limit the size of the error; this particular thermocouple is intended to verify the constant-temperature hypothesis during a pre-control phase of the experimental parameters.

6. Influence of the presence of the heat flowmeter on the determination of thermal effusivity

6.1. Problem context

The presence of the heat flowmeter serves to modify the temperature field inside the device. Considering the design of the heat flowmeter used, the two following hypotheses for modeling their behavior have been selected:

- a thermal heat flowmeter is assimilated into a homogeneous layer of apparent thermal resistance R_f and calorific capacity C_f, and
- a sensor, capable of reading in any state, represents the instantaneous flow through the middle plane of the heat flowmeter.

The temperature field in the heat flowmeter, with thickness e_f is denoted by $T_f(y, t)$ and the surfacic flow by $\varphi_f(y, t)$.

As indicated in Fig. 13, the two experimentally-accessible signals are the flow in the middle plane of the heat flowmeter $\varphi_f(0, t)$ and the temperature $T_f(e_f/2, t)$ on the surface of the sample in contact with this heat flowmeter. The problem then consists of determining, on the basis of these two indicators, the incoming heat flow through the lower face of the sample couple.

6.2. Resolution of the problem

Variable components of both the temperature field $T_f(y, t)$ and the surfacic flow $\varphi_f(y, t)$ in the heat flowmeter provide a solution to the following system of simultaneous equations:

$$\frac{\partial T_f(y,t)}{\partial t} = a_f \frac{\partial^2 T_f(y,t)}{\partial y^2} \tag{20}$$

$$T_f\left(\frac{e_f}{2}, t\right) = T(e_i + e_s, t) = |T_i| + T_i \sin(\omega t) \tag{21}$$

$$\varphi_f(0,t) = -k_f\left(\frac{\partial T_f(y,t)}{\partial y}\right)_{y=0} = |\varphi_f| \sin(\omega t + \alpha) \tag{22}$$

$$\varphi_f\left(\frac{e_f}{2}, t\right) = \varphi(e_i + e_s, t) \tag{23}$$

with a_f *and* k_f representing the equivalent thermal diffusivity and conductivity of the heat flowmeter, respectively, and e_f its thickness.

The established periodic state, which is the solution to this system, can then be written as (24):

$$\varphi_f\left(\frac{e_f}{2}, t\right) = \varphi(e_i + e_s, t) = r\,|\varphi_f| \sin(\omega t + \alpha + \gamma) \tag{24}$$

with:

$$r = \sqrt{1 - H\sin(\alpha) + \frac{H^2}{4}} \quad \text{with} \quad H = \omega C_f \frac{|T_i|}{|\varphi_f|} \tag{25}$$

$$\gamma = -\frac{H}{2}\cos(\alpha) - \frac{H^2}{4}\sin(2\alpha) - \frac{\omega R_f C_f}{8} \tag{26}$$

which enables deriving the new expression for the thermal effusivity b given by (26):

$$b = r\frac{|\varphi_f|}{|T_i|}\frac{1}{\sqrt{\omega}\chi(z)} = r b_{nc} \tag{26}$$

with b_{nc} being the value of the thermal effusivity before correction.While such a correction turns out to be vital in the case of an insulating material like polystyrene ($r \approx 0.60$), it is absolutely useless for marble. These results can be explained by the significance of the ratio C_f/b_{nc} within the correction. The parameter H can indeed be expressed in the form given by (27):

$$H = \frac{\sqrt{\omega}}{\chi(\eta)}\frac{C_f}{b_{nc}} \tag{27}$$

In the case of the marble, operations carried out around $\eta = 1.8$ make it possible to determine the thermal diffusivity and effusivity with a good level of accuracy, while maintaining the corrective coefficient r equal to 1, which yields a period of 30 min for a 5-cm thick sample.

In contrast, for the polystyrene, the zone with the most accurate measurement of effusivity is the one with the highest correction due to the flowmeter.

7. Experimental results

For the various series of tests carried out, two materials possessing very distinct thermal properties have been employed: expanded polystyrene and marble. The

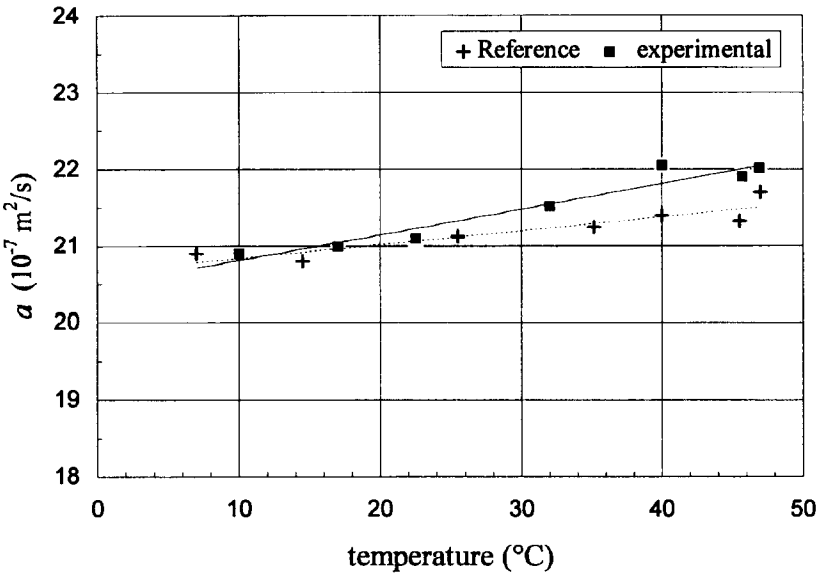

Fig. 14. Evolution of the thermal diffusivity as a function of temperature: expanded polystyrene.

samples used were 5 cm thick, and the period of the signal was set at 30 min.

By adopting an operating schedule of one day for the tests on marble and a half-day for those on polystyrene, it has been verified that the constant-temperature condition on the upper face of the sample couple is respected. Thus, it has been possible both to remove the thermocouple fixed onto the upper face and to eliminate the influence of the contact resistance between the sample couple and the upper exchanging plate.

All of the results presented in this section concern tests conducted on samples with a similar thickness ($\delta = 0.5$), which enables applying the theoretical model described in Section 3, even in the presence of contact resistance between the two samples.

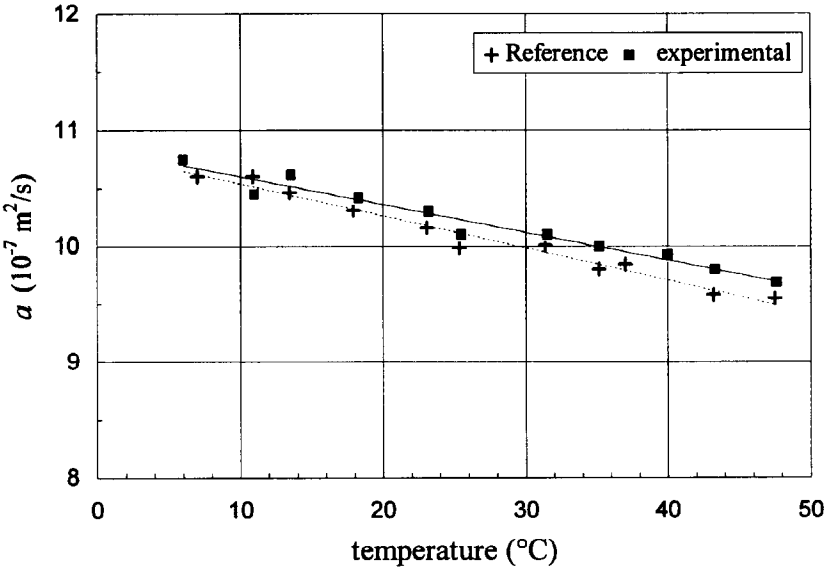

Fig. 15. Evolution of the thermal diffusivity as a function of temperature: marble.

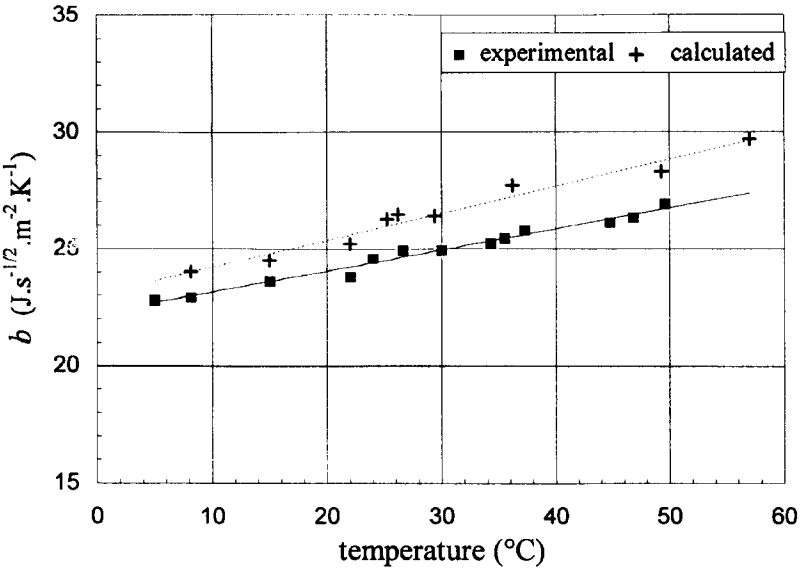

Fig. 16. Evolution of the thermal effusivity as a function of temperature: expanded polystyrene.

Thus, in order to minimize the correction necessary in the determination of thermal effusivity, the 'tangential gradient'-type of flowmeter has been used.

In the different figures, results of the thermal diffusivity and effusivity are function of the average temperature. Exploited temperature ranges are those of building's walls in tempered climates. Temperatures of tested material remain understood between 0 and 50°C; for a same test in unsteady state, the temperature difference between the two faces of the sample does not exceed 10°C.

7.1. Determination of the thermal diffusivity

In order to provide a reference against which our experimental results can be compared, the thermal diffusivity of the samples was first measured by employing a method developed previously [15]. For the two ma-

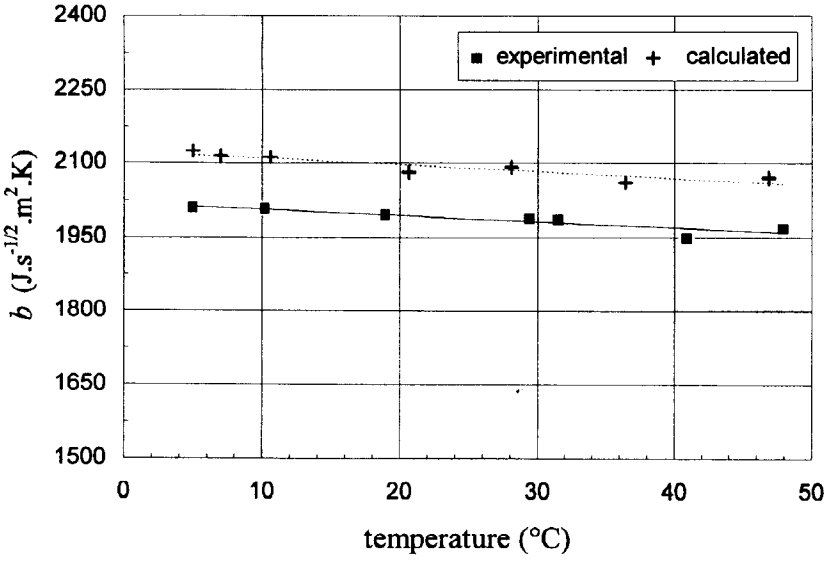

Fig. 17. Evolution of the thermal effusivity as a function of temperature: marble.

terials tested, Figs. 14 and 15 display the evolution of the thermal diffusivity as a function of temperature for both the polystyrene and the marble, respectively. Over the studied temperature range, it can be noticed that the two methods yield analogous results; nevertheless, a 2% deviation has been recorded in the case of the expanded polystyrene. Considering the operative precautions taken, it would be reasonable to estimate the accuracy of the diffusivity measurement by means of the method described herein at approximately 6%.

7.2. Determination of the thermal effusivity

From measurements of both thermal conductivity and diffusivity, it is possible to compute the effusivity b by $b = (k/\sqrt{a})$. This value has been taken as the reference, by virtue of having measured beforehand the conductivity, using the standardized, guarded hot-plate method, and the diffusivity with the method cited previously [15].

Figs. 16 and 17 exhibit the evolution of the thermal effusivity as a function of temperature for both the polystyrene and the marble, respectively. These figures enable comparing the results obtained by our method with those computed using the formula: $(k/\sqrt{a})$.

In the case of the marble, a maximal deviation of 4.5% has been observed, while this deviation can reach 15% for the polystyrene.

This sizable deviation for insulating materials can be explained, as pointed out in Section 6, by the perturbation induced from the presence of the heat flowmeter, thereby necessitating the application of a significant correction factor to the measured value. It would therefore be desirable, for this type of material, to use a heat flowmeter with a lower calorific capacity.

8. Conclusion

The experiment performed herein has proved to be quite well-suited to non-homogeneous building materials; moreover, it requires the same components as those used in the standardized, guarded hot-plate method.

The work carried out has enabled both evaluating the relative importance of the various experimental parameters involved and defining the most effective range of measurement for the different tests. It has also shown how measuring the contact resistance can be performed unsuccessfully as well as what the influence of the presence of the heat flowmeter may be on thermal effusivity results.

These measurements have allowed computing the thermal diffusivity with a high degree of accuracy, thanks to an experimental set-up that is as easy to assemble as the one obtained from the periodic state methods developed previously. A determination of thermal effusivity can also be obtained, in the case of conductor materials, with good accuracy, while in the case of insulating materials, the relevance of the results is closely tied to the performance of the heat flowmeter used. In this case, it would be appropriate to use a heat flowmeter with a lower calorific capacity.

References

[1] A. Degiovanni, Diffusivité et méthode flash, Revue Générale de Thermique 185 (1977) 420–427.
[2] A. Mokhtari, C. Martin, Diffusivité thermique des matériaux multicouches. Application à la détermination directe de la diffusivité d'un dépôt sur un substrat, Congrès Société Française des Thermiciens 1995.
[3] A. Vianou, A. Girardey, Diffusivité thermique des matériaux de construction. Mesure par la méthode du régime régulier, Revue Générale de Thermique 185 (1991) 233–239.
[4] J.C. Maréchal, J.M. Devisme, Métrologie thermique des matériaux isolants par mesure de flux en régime transitoire. Cas du système plan à températures imposées, Matériaux de construction 7 (41) (1974) 1–8.
[5] R.D. Cowan, Proposed method of measuring thermal diffusivity at high temperatures, Journal of Applied Physics 32 (7) (1961).
[6] H. Helali, M. Laurent, C. Fort, Measurement of the thermal diffusivity at very high temperatures, High Temperatures–High Pressures 26 (1994) 317–321.
[7] Norme Française X 10-021, Matéraiux faiblement conducteurs. Détermination de la conductivité thermique. Méthode de la plaque chaude gardée avec échantillons symétriques, AFNOR, Paris 1972.
[8] Norme ISO 8302-1991, Isolation thermique. Détermination de la résistance thermique et des propriétés annexes en régime stationnaire. Méthode de la plaque chaude gardée 1991.
[9] J.M. Roucoult, J.M. Devisme, T. Langlet, Mesure simultanée de la diffusivité et de l'effusivité thermiques des matériaux de construction, Annales de l'Institut Technique du Bâtiment et Travaux Publics 430 (1985) 2–11.
[10] J.M. Roucoult, J.M. Devisme, T. Langlet, Détermination simultanée de trois caractéristiques thermophysiques des matériaux de construction par une méthode de régime périodique, Annales de l'Institut Technique du Bâtiment et Travaux Publics 482 (1990) 14–23.
[11] O. Douzane, J.M. Roucoult, T. Langlet, Metrology of the thermophysical characteristics of building materials: new experimental device, High Temperatures–High Pressures 29 (1997) 443–447.
[12] M. Degenne, J.L. Magalhaes, C. Langlais, S. Klasfeld, Capteurs fluxmétriques à couches métalliques minces, Proceedings of Journées Société Française des Thermiciens 1988.
[13] T.Langlet, Contribution aux mesures fluxmétriques et à

leurs applications pour la thermique du bâtiment, Thèse de Doctorat, Université de Picardie Jules Verne, Amiens, France, 1990.

[14] J. Virgone, R. Yezou, J.J. Roux, Computer simulation of measurement error with the guarded hot plate system, in: Proceedings of the Fourteenth European Conference on Thermophysical Properties, Lyon, France, 1996, p. 315.

[15] J.C. Maréchal, J.M. Devisme, Diffusivité thermique des matériaux de construction: méthode du signal périodique, Annales de l'Institut Technique du Bâtiment et Travaux Publics 157 (1978) 82–91.